PROCEEDINGS OF SPIE

SPIEDigitalLibrary.org/conference-proceedings-of-spie

Finite difference time domain modeling of wavefront aberrations in bone using second harmonic generation microscopy

Kayvan Forouhesh Tehrani, Sendy Phang, Peter Kner, Ana Vukovic, Luke J. Mortensen

Kayvan Forouhesh Tehrani, Sendy Phang, Peter Kner, Ana Vukovic, Luke J. Mortensen, "Finite difference time domain modeling of wavefront aberrations in bone using second harmonic generation microscopy," Proc. SPIE 10502, Adaptive Optics and Wavefront Control for Biological Systems IV, 105020R (23 April 2018); doi: 10.1117/12.2290376



Event: SPIE BiOS, 2018, San Francisco, California, United States

Finite Difference Time Domain modeling of wavefront aberrations in bone using second harmonic generation microscopy

Kayvan Forouhesh Tehrani, ¹ Sendy Phang, ² Peter Kner, ³ Ana Vukovic, ⁴ Luke J. Mortensen ^{1,3,*}

¹Regenerative Bioscience Center, Rhodes Center for ADS, University of Georgia, Athens, GA 30602, USA; ²School of Mathematical Sciences, University of Nottingham, Nottingham NG7 2RD, UK; ³College of Engineering, University of Georgia, Athens, GA 30602, USA; ⁴George Green Institute for Electromagnetics Research, University of Nottingham, Nottingham NG7 2RD, UK

ABSTRACT

Near infrared and infrared multi-photon imaging through or inside bone is an emerging field that promises to help answer many biological questions that require minimally invasive intravital imaging. Neuroscience researchers especially have begun to take advantage of long wavelength imaging to overcome multiple scattering and image deep inside the brain through intact or partially intact bone. Since the murine model is used in many biological experiments, here we investigate the optical aberrations caused by mouse cranial bone, and their effects on light propagation. We previously developed a ray tracing model that uses second harmonic generation in collagen fibers of bone to estimate the refractive index structure of the sample. This technique is able to rapidly provide initial information for a closed loop adaptive optics system. However, the ray tracing method does not account for refraction or scattering. Here, we extend our work to investigate the wavefront aberrations in bone using a full electromagnetic model. We used Finite-Difference Time-Domain modeling of light propagation in refractive index bone datasets acquired with second harmonic generation imaging. In this paper we show modeled wavefront phase from different originating points across the field of view.

Keywords: Adaptive Optics, Aberrations, Scattering, Multi-photon microscopy, Second Harmonic Generation.

1. INTRODUCTION

Scattering and optical refractive index variations distort imaging quality, and severely reduce the resolution and penetration of deep tissue imaging. Multi-photon microscopy [1] partially overcomes these challenges through the use of near-infrared excitation light, which suffers less from scattering than the visible wavelengths used for single photon imaging. Multi-photon microscopy through intact bone or thinned bone is important for many biological studies in bone research [2], neuroscience [3], and many other fields of research [4], but imaging through bone is still very challenging. The highly scattering nature of bone causes the light beam to deviate from the diffraction-limited state and causes the point spread function (PSF) to be spread over a larger volume with a distorted shape, lowering the efficiency of the multi-photon excitation as well as the resolution of the imaging. Scattering in a medium is caused by particles and features close-to and smaller than the wavelength of light. Bone is constructed of many layers of collagen fibers with different orientations. The collagen fibers are made of many nano-fibers with radii in the range of 100-500 nm [5] which therefore, due to their sub-wavelength size, scatter light strongly. We previously developed a technique called Phase Accumulation Ray Tracing (PART) [6] to characterize the optical aberrations caused by bone. This method produces an estimate of bone aberrations by acquiring Second Harmonic Generation (SHG) images of the bone, scaling them to the refractive index, and calculating the phase accumulation by ray

Adaptive Optics and Wavefront Control for Biological Systems IV, edited by Thomas G. Bifano, Joel Kubby, Sylvain Gigan, Proc. of SPIE Vol. 10502, 105020R ⋅ © 2018 SPIE ⋅ CCC code: 1605-7422/18/\$18 ⋅ doi: 10.1117/12.2290376

^{*} Luke.mortensen@uga.edu

tracing from the point source to the pupil. PART can be used to produce an initial input for an iterative Adaptive Optics (AO) correction algorithm. Although PART is very fast in producing analytical information, it does not take into account scattering and refraction inside of the tissue, due to phase accumulation. To overcome this problem, we performed Finite Difference Time Domain (FDTD) analysis of light propagation in bone to study other distortions and optical effects. In this paper we show FDTD simulations of points sources placed on a 3×3 grid with 7.5 μm spacing below the layer of bone (Fig. 1). We produce point sources that emulate the diffraction-limited PSF of our microscope, we then perform the time-reversed propagation of light in the tissue, which yields the distribution of the electric field at the pupil. Based on these results we calculate the wavefront phase for each originating point.

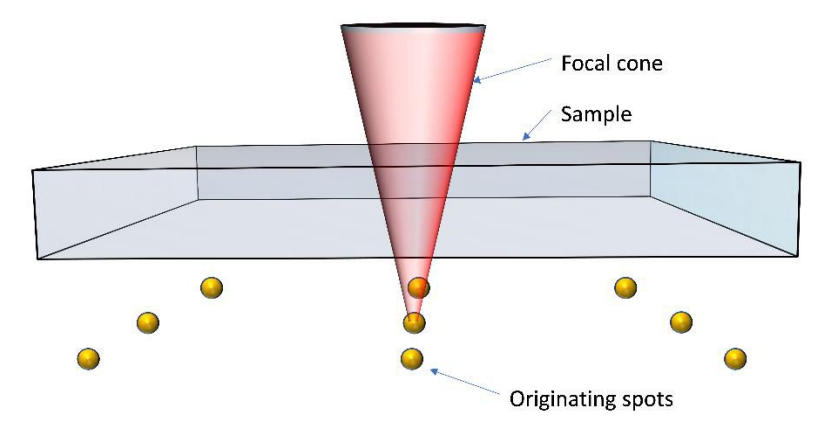


Figure 1 - Schematic illustration of the sample and locations of the point sources. The sample is $35 \, \mu m \times 35 \, \mu m \times 25 \, \mu m \, (x,y,z)$ and the point sources are placed 7.5 $\, \mu m$ apart from each other.

2. METHODS

2.1 Imaging Apparatus

We used our 2-photon microscope, which is a home-built setup based on our previous efforts [7, 8]. A 1550 nm, 370 femtosecond pulsed fiber laser (Calmar Cazadero) with wavelength of 1550 nm and repetition rate of 10 MHz was used. The beam was frequency doubled with a second harmonic generation (SHG) crystal (Newlight Photonics) to produce a 775 nm beam for 2-photon excitation of the sample. Power was modulated using a Pockels cell (Conoptics) and scanned over the sample by a resonant-galvanometer (fast axis – slow axis) scanner (Sutter instruments MDR-R). A 60x Olympus (LUMFLN60x) water immersion objective with NA of 1.1 was used for imaging. Z-scanning was performed using an X-Y-Z stage from the Sutter Instruments (MPC-200). Emitted SHG signal from the sample was collected using a 390/18 nm filter (Semrock). Photon Multiplier Tubes from Hamamatsu (H10770-40) were used for collection of the signal, and their signal amplified with a transimpedance amplifier (Edmund Optics 59-178). The system is capable of simultaneous 3 color imaging, but in these experiments, we only used one channel for acquisition. A National Instruments DAQ card and FPGA module were used for control and synchronization of the system, and digitizing of the amplified SHG signal. The MATLAB-based Open-source software, Scanimage [9] was employed to control the microscope.

2.2 Simulation

We use a commercially available FDTD [10] numerical package to give a full-wave vectorial analysis of a Gaussian light beam diverging through a scattering layer of bone (to simulate a time-reversed focus). The

linear and isotropic refractive indices are calculated using the method described in section 2.3 and given to the FDTD simulation. The FDTD simulation is performed for a volume of tissue $35 \times 35 \times 25 \ \mu m$ (x, y, z) with sample resolution of $73.5 \times 73.5 \times 100 \ nm$ (dx, dy, dz). The FDTD simulation has a uniform spatial discretization of $\Delta \ell = \lambda_{\rm op}/(10 n_{\rm max})$. To emulate the actual PSF of our microscope, the beam is operated at free-space wavelength $\lambda_{\rm op} = 775 \ \rm nm$ with 30 nm bandwidth, centered at $\lambda_{\rm op}$ and beam's focus waist diameter ($1/e^2$ power) is $w = 326 \ \rm nm$, i.e. NA = 1.1. The beam is launched with focal spot located at a fixed distance of $z = 1 \ \mu m$ beneath the sample. The sample is assumed to be immersed in a PBS solution with refractive index $n_{\rm bg} = 1.33$. Perfectly Matched Layer (PML) is used on all computational domain boundaries to avoid unwanted reflection at the boundary.

The temporal simulation results are recorded by a monitor plane at the sample surface (above the bone layer). The stationary response is obtained by performing a Fourier transform of the temporal dataset at λ_{op} , upon which the electric field intensity $|E(\lambda_{op})|^2$ is then calculated.

2.3 Refractive Index Calculation

We calculate the indices of refraction for each point using

$$n = \begin{cases} k_2 \sqrt{I_{2\omega} - I_b} + n_{\min} & I > I_b \\ n_b & otherwise \end{cases}, \tag{1}$$

where $I_{2\omega}$ is the SHG intensity, I_b is intensity of background, n_{\min} and n_b are minimum refractive index of bone, and refractive index of background medium, respectively. k_2 is a parameter found empirically that relates intensity of SHG to n. In this study the range for the bone indices were chosen from 1.528 to 1.604 [11], and a refractive index of 1.33 was used for the n_b . These values are normalized for depth, to correct for attenuations due to depth. For more details on this method please refer to [6, 12].

3. RESULTS

Here we show the results of our simulations. We calculated the relative transmittance by dividing the transmitted light intensity in presence of bone, by the Gaussian beam when the sample is replaced with a homogenous media (phosphate buffered saline n=1.33), as depicted in figure 2. We further show the phase of the relative transmittance for different beam focal point positions (Fig. 3). Our results show a range of about $\phi \approx \pi$ of distortion in the extreme case.

4. CONCLUSION

In conclusion we showed FDTD simulation of light propagation in a sample that is $25 \,\mu m$ thick. We used our previously reported [6, 12] method to scale the second harmonic generation signals to the refractive indices of the sample. Because the thickness of the sample is less than one mean-free-path we did not expect large optical distortions, however our findings show that there exists high order scattering that needs to be corrected to produce diffraction-limited resolution.

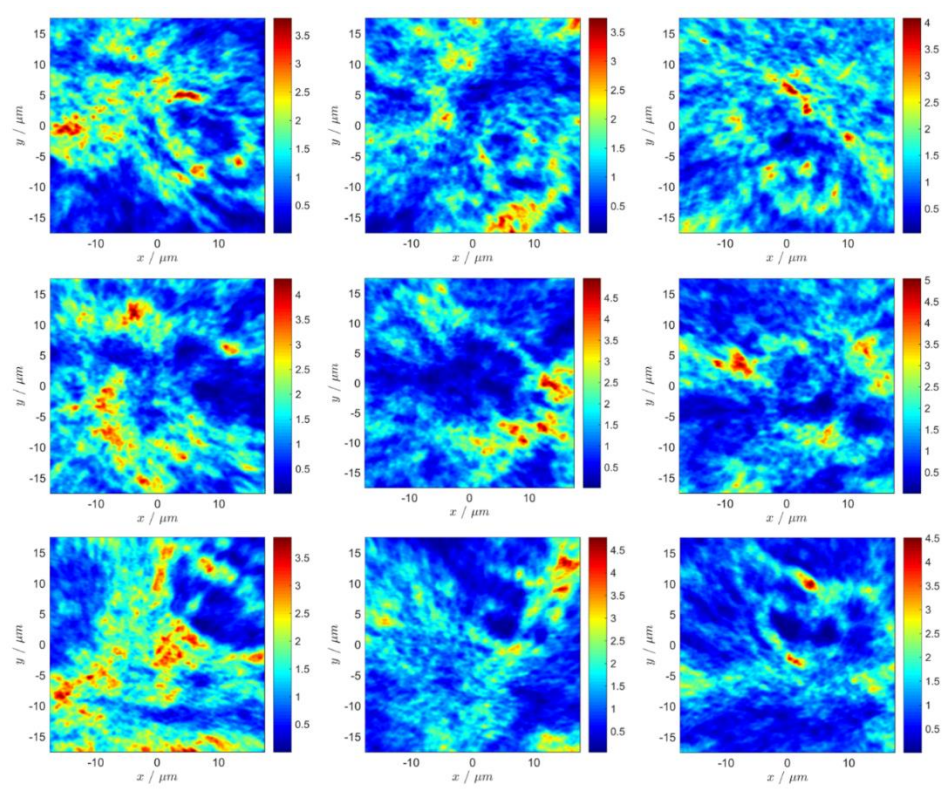


Figure 2 - Relative transmittance of light propagation through bone, obtained from the FDTD simulation. Each panel corresponds to an originating point on the 3 x 3 grid at the bottom of the sample.

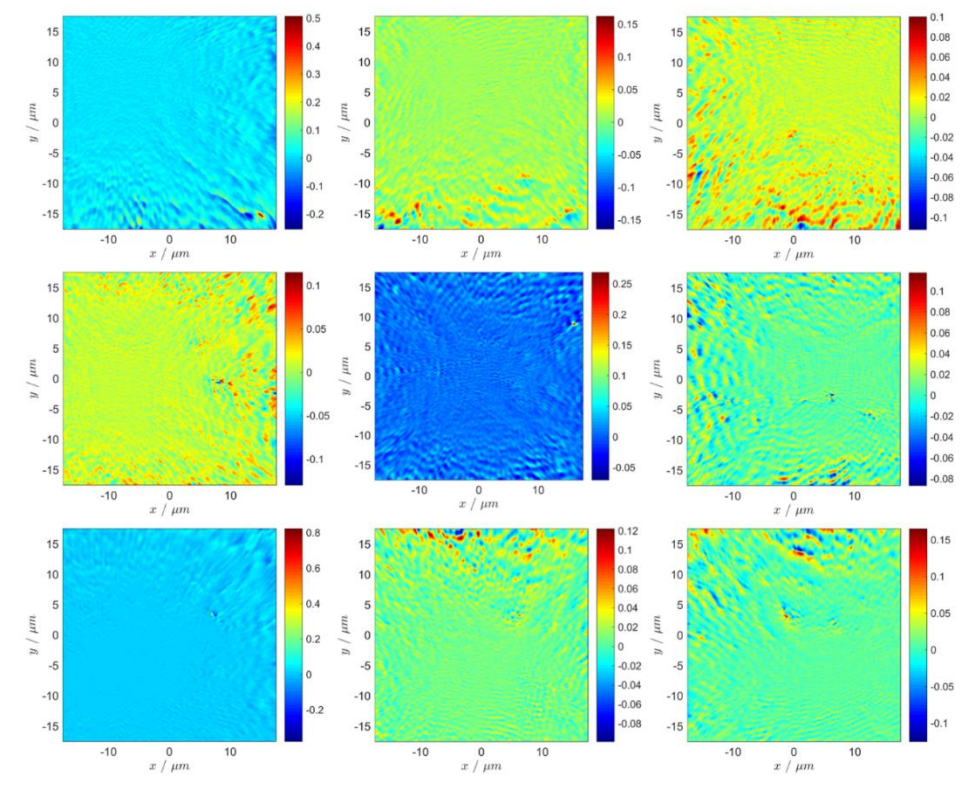


Figure 3 – Normalized phase of the relative transmittance ($\angle T/\pi$).

5. ACKNOWLEDGEMENTS

We acknowledge National Science foundation grant 1706916 to LJM and PK, Georgia Partners in Medicine REM seed grant, and Georgia Tech Marcus Center Grant to LJM. SP acknowledges the support of the European Commission for NEMF21 project; under the framework Horizon 2020 Future Emerging Technologies (FET) grant No. 664828.

6. REFERENCES

- [1] W. Denk, J. Strickler, and W. Webb, "Two-photon laser scanning fluorescence microscopy," Science, 248(4951), 73-76 (1990).
- [2] R. Turcotte, C. Alt, L. J. Mortensen *et al.*, "Characterization of multiphoton microscopy in the bone marrow following intravital laser osteotomy," Biomedical Optics Express, 5(10), 3578-3588 (2014).
- [3] K. Wang, W. Sun, C. T. Richie *et al.*, "Direct wavefront sensing for high-resolution in vivo imaging in scattering tissue," Nat Commun, 6, (2015).
- [4] K. F. Tehrani, E. G. Pendleton, W. M. Southern *et al.*, "Two-photon deep-tissue spatially resolved mitochondrial imaging using membrane potential fluorescence fluctuations," Biomedical Optics Express, 9(1), 254-259 (2018).
- [5] K. S. Rho, L. Jeong, G. Lee *et al.*, "Electrospinning of collagen nanofibers: Effects on the behavior of normal human keratinocytes and early-stage wound healing," Biomaterials, 27(8), 1452-1461 (2006).
- [6] K. F. Tehrani, P. Kner, and L. J. Mortensen, "Characterization of wavefront errors in mouse cranial bone using second-harmonic generation," Journal of Biomedical Optics, 22(3), 036012-036012 (2017).
- [7] L. J. Mortensen, C. Alt, R. Turcotte *et al.*, "Femtosecond laser bone ablation with a high repetition rate fiber laser source," Biomedical Optics Express, 6(1), 32-42 (2015).
- [8] K. F. Tehrani, E. G. Pendleton, C. P. Lin *et al.*, "Deep tissue single cell MSC ablation using a fiber laser source to evaluate therapeutic potential in osteogenesis imperfecta," Proc. SPIE. 9711, 97110D-97110D-8 (2016).
- [9] T. A. Pologruto, B. L. Sabatini, and K. Svoboda, "ScanImage: flexible software for operating laser scanning microscopes," Biomed Eng Online, 2, 13 (2003).
- [10] [Solutions F. D. T. D.] Lumerical Solutions. Inc., (2003).
- [11] A. Ascenzi, and C. Fabry, "Technique for Dissection and Measurement of Refractive Index of Osteones," The Journal of Biophysical and Biochemical Cytology, 6(1), 139-142 (1959).
- [12] K. Tehrani, P. Kner, and L. J. Mortensen, "Modelling of optical aberrations caused by light propagation in mouse cranial bone using second harmonic generation imaging," Proc. SPIE. 10073, 100731F-100731F-7 (2017).